PROCEEDINGS OF SCIENCE

Higgs properties and supersymmetry

F. Mahmoudi*

Université de Lyon, Université Claude Bernard Lyon 1, CNRS/IN2P3,
Institut de Physique des 2 Infinis de Lyon, UMR 5822, F-69622, Villeurbanne, France

Theoretical Physics Department, CERN, CH-1211 Geneva 23, Switzerland

E-mail: nazila@cern.ch

The exploration of the properties of the Higgs boson presents compelling opportunities to test the effects of new physics beyond the Standard Model. By accurately determining the properties of the Higgs boson, we can gain a highly precise understanding of the Higgs sector, establish stringent constraints, and predict potential ranges for new physics model parameters. This contribution focuses on examining the constraints imposed on supersymmetry by analyzing the mass and couplings of the Higgs boson. We conduct scans across the 19-parameter space of the phenomenological minimal supersymmetric Standard Model. We investigate the fraction of scan points that can be excluded based on Higgs measurements, considering the precision of coupling measurements achieved during LHC Run 2, the anticipated precision for the HL-LHC program, as well as e^+e^- colliders. These findings are then compared with constraints derived from searches for missing transverse energy at the LHC and from experiments related to dark matter.

Corfu Summer Institute 2022 "School and Workshops on Elementary Particle Physics and Gravity",
28 August - 1 October, 2022
Corfu, Greece

*Speaker

PoS(CORFU2022)075

1. Introduction

The discovery of the Higgs boson [1] at the LHC [2] has allowed for extensive studies of its properties and provided constraints on new physics models. Supersymmetric models have been of particular interest, as they offer an extended particle spectrum and an expanded Higgs sector. Although current LHC studies have placed stringent bounds on the masses of new particles, supersymmetry remains a valuable benchmark for new physics searches. Precise measurements of the Higgs boson's mass and its couplings to Standard Model (SM) particles are crucial for understanding electroweak symmetry breaking, exploring new physics contributions, and setting constraints on parameter spaces. These constraints must be compared with direct searches for heavier Higgs bosons and supersymmetric particles. The LHC experiments have already established significant limits, and future runs will continue to probe heavier supersymmetric particles. Understanding the interplay between Higgs physics and supersymmetry, as well as the impact of Higgs measurements on parameter reconstruction, is essential. The future e^+e^- collider, following the LHC era, will provide more precise measurements covering all Higgs decay channels. This contribution addresses these issues by studying the relationship between Higgs coupling modifiers and fundamental supersymmetric parameters, as well as the sensitivity of Higgs measurements to supersymmetry. The study focuses on the phenomenological Minimal Supersymmetric extension of the Standard Model (pMSSM) [3] and compares the constraints derived from Higgs properties with those from direct supersymmetry searches, flavour physics, and dark matter searches. We refer the reader to [4] for more details on the analysis and references.

2. Higgs Properties in the pMSSM

In the MSSM, the presence of two doublets of complex scalar fields, H_u and H_d, is necessary to spontaneously break the electroweak symmetry. This results in five Higgs states: two CP-even Higgs bosons (h and H, with h considered the lightest), a CP-odd Higgs state (A), and two charged Higgs bosons ($H^\pm$). The masses and couplings of these Higgs bosons in the MSSM depend mainly on two input parameters: the pseudoscalar Higgs mass (M_A) and the ratio of the two vacuum expectation values ($\tan\beta$). However, the radiative corrections to the Higgs sector involve many other MSSM parameters, which are known to be crucial.

For the analysis of the Higgs sector, we adopt the pMSSM framework. This framework assumes that all soft SUSY-breaking parameters are real, there is no new source of CP-violation, the matrices for sfermion masses and trilinear couplings are diagonal (implying no flavour change at tree level), and the soft SUSY-breaking masses and trilinear couplings of the first and second sfermion generations are the same at the electroweak symmetry breaking scale. By making these assumptions, the pMSSM reduces the number of input parameters to 22. These parameters include $\tan\beta$, M_A, μ, M_1, M_2, M_3, $m_{\tilde{Q}}, m_{\tilde{t}_R}, m_{\tilde{b}_R}, m_{\tilde{L}}, m_{\tilde{\tau}_R}$, A_t, A_b, A_τ, and $m_{\tilde{q}}, m_{\tilde{u}_R}, m_{\tilde{d}_R}, m_{\tilde{l}}, m_{\tilde{e}_R}$ representing the trilinear couplings and mass parameters of various SUSY particles.

In most cases, the first and second generation trilinear couplings (A_u, A_d, and A_e) have minimal significance and can be ignored or equated to those of the third generation, resulting in a practical model with 19 basic parameters. This approach enhances predictability and provides a suitable and generic framework for comprehensive phenomenological studies in the MSSM.

3. Higgs couplings

The tree-level couplings of the neutral MSSM Higgs bosons to the up-quarks, down-quarks and charged leptons and vector bosons normalised to SM are given in Table 1 as functions of the Higgs mixing angle α and β. The decoupling limit is reached for large M_A such that $-\sin\alpha/\cos\beta \to 1$, and the light Higgs couplings become equal to the SM Higgs ones.

ϕ	$g_{\phi u\bar{u}}$	$g_{\phi d\bar{d}} = g_{\phi \ell\bar{\ell}}$	$g_{\Phi VV}$
h	$\cos\alpha/\sin\beta \to 1$	$-\sin\alpha/\cos\beta \to 1$	$\sin(\beta-\alpha) \to 1$
H	$\sin\alpha/\sin\beta \to -\cot\beta$	$\cos\alpha/\cos\beta \to \tan\beta$	$\cos(\beta-\alpha) \to 0$
A	$\cot\beta$	$\tan\beta$	0

Table 1: MSSM tree level Higgs couplings relative to the SM couplings. The arrows give the values in the decoupling limit corresponding to $M_A \gg M_Z$.

The Higgs couplings can however be modified by QCD and EW corrections involving SUSY particles in the loops, and in particular [5, 6]:

$$g^{\text{eff}}_{hf\bar{f}} = \frac{g_{hf\bar{f}}}{1+\Delta_f}\left[1 - \frac{\Delta_f}{\tan\alpha\tan\beta}\right], \quad (1)$$

$$g^{\text{eff}}_{Hf\bar{f}} = \frac{g_{Hf\bar{f}}}{1+\Delta_f}\left[1 + \Delta_f\frac{\tan\alpha}{\tan\beta}\right], \quad (2)$$

$$g^{\text{eff}}_{Af\bar{f}} = \frac{g_{Af\bar{f}}}{1+\Delta_f}\left[1 - \frac{\Delta_f}{\tan^2\beta}\right], \quad (3)$$

where f stands for fermions and Δ_f incorporates the QCD and EW corrections. The SUSY-QCD corrections can make $|\Delta_f| \sim 1$.

The LHC has provided measurements of the Higgs couplings. Table 2 shows a summary of the experimental measurements and projections for the coupling modifiers, i.e. effective Higgs couplings normalised to their SM values, which have been determined from the production and decay rates in many different channels measured at the LHC.

In the following, we discuss the possibilities to distinguish the MSSM Higgs from the SM Higgs.

4. LHC constraints and pMSSM

We perform flat scans over the pMSSM 19 parameters varying all the masses between 0 and 6 TeV, the trilinear couplings between -15 and 15 TeV, and $\tan\beta$ between 1 and 60 [8]. The master program is based on SuperIso [9], we generate the MSSM spectra with SOFTSUSY [10] and compute the Higgs boson decay widths and couplings with HDECAY [11], and dark matter related observables with SuperIso Relic [12]. We keep only the parameter points for which the lightest supersymmetric particle is a neutralino (constituting a dark matter candidate) and a light Higgs mass of 125 ± 2 GeV.

We first study the effect of experimental selections from LHC high-p_T searches. For this purpose, we use many different SUSY and Higgs search channels in order to assess whether a

Coupling modifier	ATLAS 13 TeV 25-79.8 fb^{-1}*	ATLAS 14 TeV 3 ab^{-1} †	ILC 250 GeV 2 ab^{-1}	ILC 1 TeV 8 ab^{-1}	FCC-ee 365 GeV 1.5 ab^{-1}
k_W	1.05 ± 0.09	± 0.022	± 0.0180	± 0.0024	± 0.0043
k_Z	1.11 ± 0.08	± 0.018	± 0.0029	± 0.0022	± 0.0017
k_t	$1.03^{+0.15}_{-0.14}$	$^{+0.043}_{-0.040}$	–	± 0.016	–
k_b	$1.09^{+0.19}_{-0.17}$	$^{+0.044}_{-0.028}$	± 0.0180	± 0.0048	± 0.067
k_τ	$1.05^{+0.16}_{-0.15}$	$^{+0.028}_{-0.027}$	± 0.0190	± 0.0057	± 0.0073
k_g	1.05 ± 0.09	$^{+0.032}_{-0.030}$	± 0.0230	± 0.0066	± 0.0100
k_γ	$0.99^{+0.11}_{-0.10}$	$^{+0.028}_{-0.023}$	± 0.0670	± 0.019	± 0.0390

Table 2: Experimental determination of the Higgs coupling modifiers. The second column corresponds to the current values determined by ATLAS, the third one to projections of the uncertainties at the end of the HL-LHC run. The next columns correspond to projections of the uncertainties at the ILC and FCC-ee [7].

pMSSM point is excluded or not. Since the pMSSM is an unconstrained scenario, the constraints on the SUSY masses are less strict than in simplified scenarios. Figure 1 shows the fractions of pMSSM points incompatible with LHC data as functions of the gluino and stop 1 masses. As can be seen in the figure, the gluinos can be as light as 1 TeV, stops as light as 400 GeV in the pMSSM, and the constraints are very loose for the pseudoscalar Higgs boson and charginos.

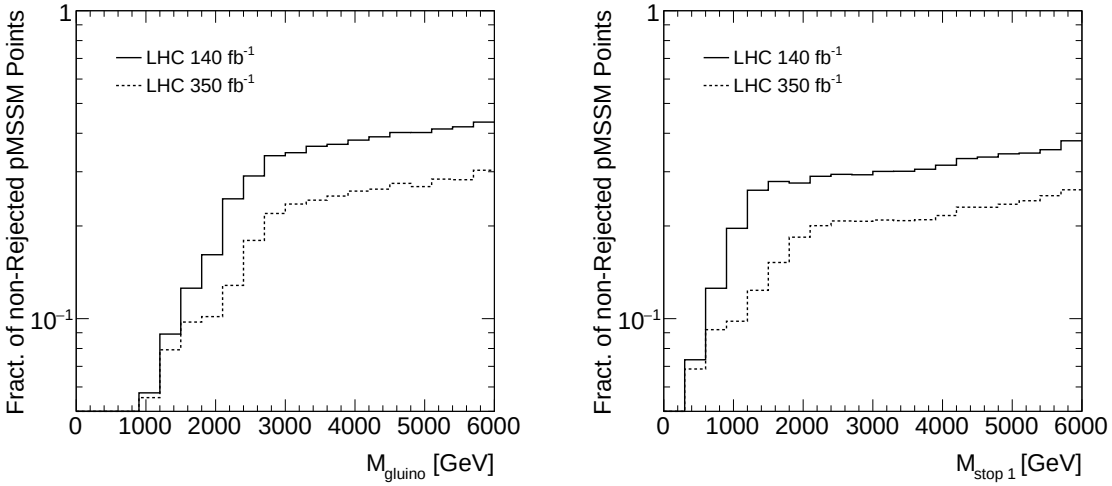

Figure 1: Fraction of pMSSM points excluded by LHC high-p_T search data, with the current 140 fb^{-1} and extrapolated to 300 fb^{-1} as a function of the gluino and stop 1 masses.

Next we consider the constraints from light Higgs coupling measurements, as given in Table 2. The branching fractions of the h bosons in our pMSSM scans in the $b\bar{b}$, W^+W^- and ZZ and $\tau^+\tau^-$ decay channels normalised to the SM predictions are shown in Figure 2. As can be seen, most of the pMSSM points have coupling modifiers in agreement with the experimental results, and κ_b varies over a large range. An important effect with significant impact on κ_b comes from the Δ_b

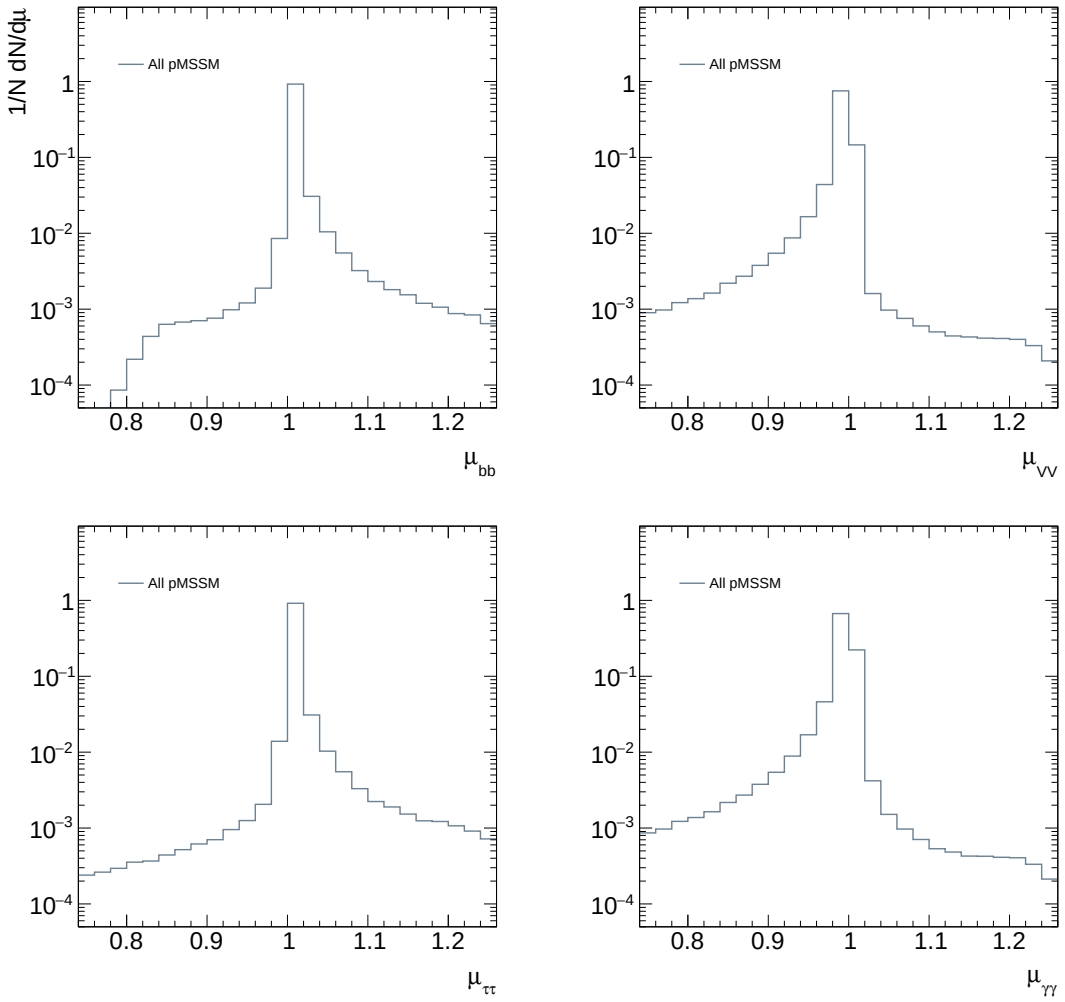

Figure 2: Distributions of h decay branching fractions normalised to their SM prediction, μ, for the $b\bar{b}$ (top), W^+W^- and ZZ (second from top), $\tau^+\tau^-$ (bottom) and $\gamma\gamma$ (second from bottom) channels for pMSSM points.

correction [13]:

$$\Delta_b \approx \frac{2\alpha_s}{3\pi} \frac{m_{\tilde{g}} \mu \tan\beta}{\max(m^2_{\tilde{g}}, m^2_{\tilde{b}_1}, m^2_{\tilde{b}_2})} + \frac{m_t^2}{8\pi^2 v^2 \sin^2\beta} \frac{A_t \mu \tan\beta}{\max(\mu^2, m^2_{\tilde{t}_1}, m^2_{\tilde{t}_2})}, \tag{4}$$

which is proportional to $\mu \tan_\beta$ and can in principle be as large as 1, in particular in the large gluino mass limit or large A_t.

However, there exists only a mild correlation between $\mu \tan\beta$ and μ_{bb}, and the small shifts are dominated by deviations of the mixing angle α from the SM limit. This is due to a suppression of the Δ_b corrections in the region of M_A still compatible with the experimental constraints.

We present a comparison of the coupling modifier distributions, κ_X, for the valid pMSSM points in our scans with those obtained for points not excluded by direct searches in Run 2 and with

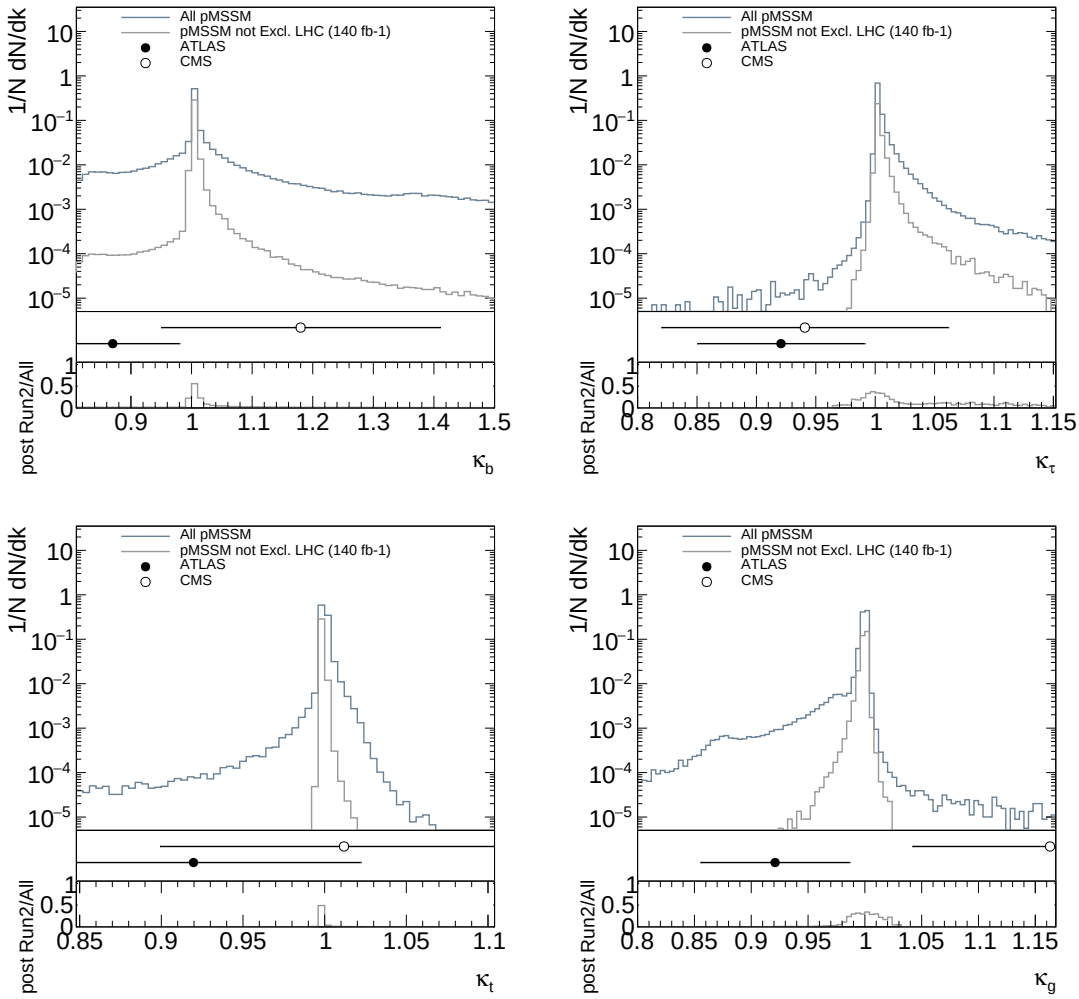

Figure 3: h Higgs boson coupling modifiers, κ_X, to b quarks (upper left), τ leptons (upper right), top quarks (lower left) and gluons (lower right) for all valid pMSSM points and those not excluded by the LHC Run 2 searches compared to the present measurements by the ATLAS [14] and CMS [15] experiments. The lower panels show the fractions of non-excluded pMSSM points as a function of κ_X.

the current experimental measurements (Figure 3). Additionally, we examine the coupling modifier values, κ_X, obtained from correlating particles using the LHC data (Figure 4). It is worth noting that the current experimental accuracy encompasses the range of predictions from the pMSSM. Thus, it can be said that the properties of the observed Higgs boson are both SM-like and MSSM-like. However, a fraction of the pMSSM solutions is found to be inconsistent with these measurements, and further testing will be carried out at the HL-LHC and potentially at an e^+e^- Higgs factory. It is interesting to investigate the coupling properties of the points that are predominantly excluded by direct searches. When comparing the distributions of κ_X for all valid pMSSM points with those not excluded by direct LHC searches for heavy Higgs bosons and SUSY particles in missing E_T channels, we observe that the preferentially excluded pMSSM points lie in the tails of the κ_i

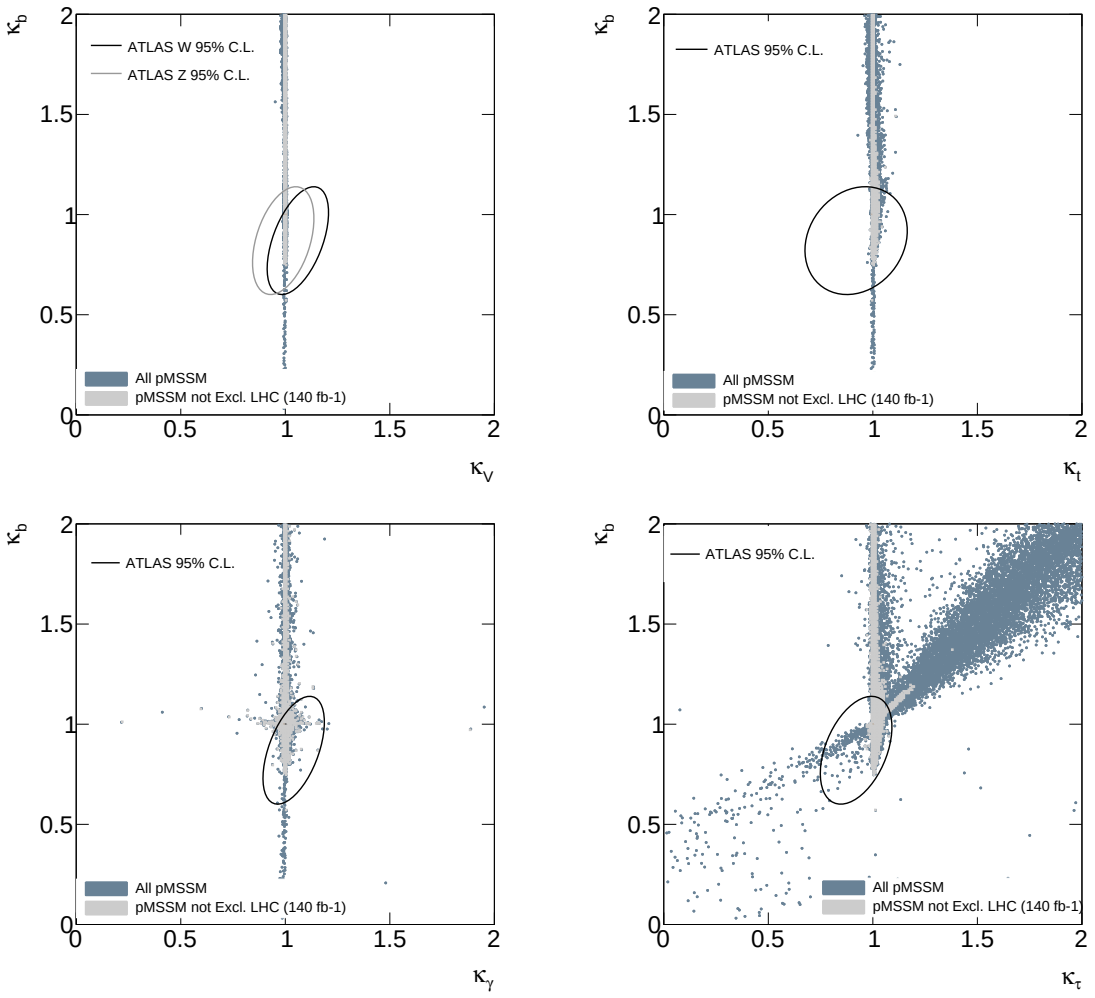

Figure 4: pMSSM valid points (dark colour) and points not excluded by LHC searches (light colour) in the κ_b vs. κ_V (upper left), κ_t (upper right), κ_γ (lower left) and κ_τ (lower right) parameter planes. Superimposed are the experimental contours at 95% C.L. of ATLAS and CMS.

distributions, deviating significantly from the SM predictions where $\kappa_X = 1$. The decrease in the number of pMSSM points at κ values substantially higher than the SM expectations for b quarks and τ leptons, caused by the SUSY searches, is primarily attributed to the constraint on M_A imposed by the $H/A \to \tau^+\tau^-$ channel searches.

5. Invisible Higgs decays and DM direct detection

If the mass of the neutralino LSP is less than half the mass of the Higgs boson, the Higgs boson can decay into pairs of neutralinos. The rate of invisible Higgs decays provides limits on the neutralino LSP mass. The coupling between the Higgs boson (h) and the neutralinos (χ) also affects the scattering cross section of neutralinos with protons (χp), creating a correlation between the decay rate of $h \to \chi\chi$, the scattering cross section, and the neutralino relic density ($\Omega_{\tilde{\chi}_1^0}$).

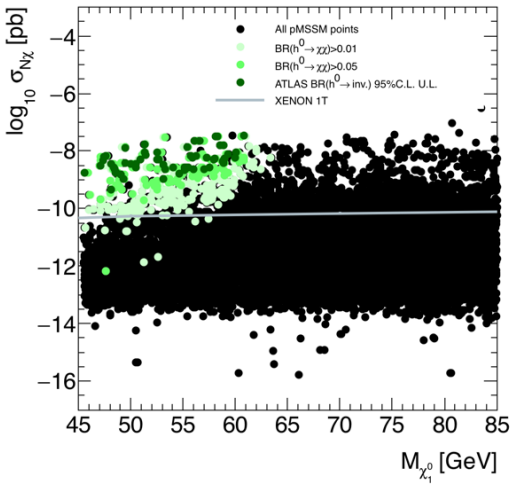

Figure 5: Predicted spin-independent χN scattering cross section on nucleons, as a function of $M_{\tilde{\chi}_1^0}$ values with highlighted pMSSM points with sizeable $h \to \chi\chi$ branching fractions. Points with sizeable $h \to \chi\chi$ branching fractions are shown in colour, the darker shade indicating those with branching fractions exceeding the ATLAS upper bounds on invisible Higgs boson decays [19]. The line represents the upper bound from the XENON-1T data [20]. The lower panel has the χN scattering cross section values rescaled by $\Omega_\chi/\Omega_{\rm CDM}$.

A higher rate of invisible Higgs decays implies a larger scattering cross section for χp due to the enhanced coupling between h and $\chi\chi$. Figure 5 illustrates the predicted spin-independent scattering cross section of neutralinos with nucleons (χN) for a subset of pMSSM points with low $M_{\tilde{\chi}_1^0}$, highlighting points with significant $h \to \chi\chi$ branching fractions. Bounds on the χ scattering cross section impose constraints on the Higgs invisible decay rate, as shown in Figure 5. Even when rescaled by the ratio $\Omega_\chi/\Omega_{\rm CDM}$ for points with lower neutralino relic density than the current PLANCK result for $\Omega_{\rm CDM}$, these bounds remain relaxed but not invalidated.

Specifically, the XENON-1T experiment's upper limit on the scattering cross section of neutralinos with nucleons, obtained from a 1.0-ton-yr exposure and applied to neutralino masses below $M_h/2$, removes the majority of MSSM solutions with a branching ratio of $h \to \chi\chi$ above 0.01. It provides a competitive constraint compared to the direct upper bound on Higgs invisible decays within the MSSM, which is 0.11 [16–19]. This is significant as the lightest neutralino is assumed to be the only source of dark matter in the MSSM.

As a result, the invisible Higgs decay rate is likely to be below the sensitivity of the LHC, determined either directly through ZH and vector boson fusion (VBF) production or indirectly through the sum of Higgs rates. This makes the measurement of the invisible Higgs decay rate unique to the e^+e^- collider program. In a pMSSM scenario with a neutralino mass of $M_\chi = 58.3$ GeV, the fit to the Higgs branching fractions enables the indirect reconstruction of the neutralino mass with a relative statistical accuracy better than 10%.

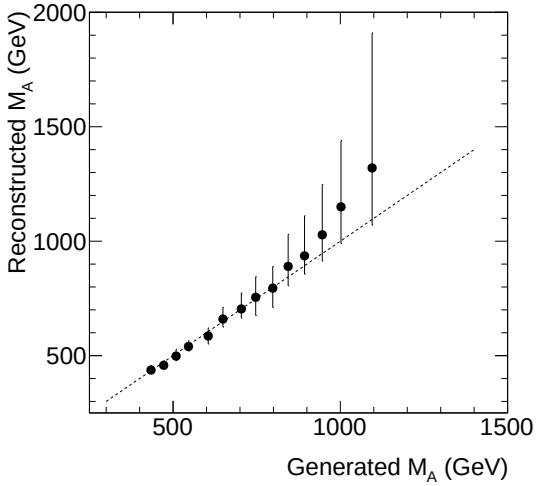

M_A (GeV)	$\tan\beta$	μ	$M_{\chi_1^0}$
434.4	5.58	-549.3	562.1
472.4	6.62	1993.7	314.8
509.8	5.48	-181.9	184.7
546.9	5.55	-50.5	49.9
605.7	6.31	369.1	380.1
649.5	3.15	1722.6	108.3
704.4	5.24	480.5	170.6
747.0	4.51	-3596.1	1072.0
798.4	5.75	-3301.7	1329.4
844.3	9.11	-1679.5	1695.1
893.2	7.14	-367.9	379.5
946.9	7.65	-4268.0	363.5
1001.9	5.39	715.9	732.0

Figure 6: Reconstruction of M_A at ILC 1 TeV from Higgs decay measurements. Details on the properties of the original pMSSM points are provided in the table.

6. Determination of SUSY parameters at ILC

We examine the possibility of reconstructing the MSSM parameters by measuring more precisely the Higgs couplings at a future Higgs factory. Considering the optimal case of an ILC with 1 TeV energy in the center of mass, we study benchmark points which are currently compatible with Higgs and SUSY direct searches, with masses as low as 434 GeV and at low $\tan\beta$ between 3 and 10. The SUSY particles do not have a significant effect on the BRs, so the main sensitivity is to M_A and $\tan\beta$.

In Figure 6 we show the reconstructed pseudoscalar Higgs mass as a function of the expected mass for all the benchmark points. The reconstruction is very precise for light M_A and the uncertainties increase with M_A, but it is still possible to reconstruct a mass of 1 TeV.

7. Summary

The study of the Higgs boson's properties provides valuable insights into physics beyond the Standard Model, particularly in supersymmetric models like the MSSM. This analysis explores how supersymmetric corrections affect the Higgs boson's couplings and decay rates, considering relevant MSSM parameters. Comparisons are made between the constraints derived from Higgs measurements and those obtained from direct searches at the LHC. The findings indicate that while the pseudoscalar Higgs mass has a significant impact, other MSSM parameters have limited influence on Higgs couplings and decay rates. The results highlight that current and future collider measurements can exclude certain MSSM scenarios and provide indirect information about the pseudoscalar Higgs mass. Overall, the observed Higgs boson's properties align not only with the Standard Model but also with characteristics of the MSSM.

Acknowledgements

I would like to thank the organisers for their invitation and for the very inspiring workshop. I am also grateful to my collaborators on this project: A. Arbey, M. Battaglia, A. Djouadi, M. Muhlleitner and M. Spira.

References

[1] P. W. Higgs, Phys. Lett. **12** (1964) 132, Phys. Rev. Lett. **13** (1964) 508 and Phys. Rev. **145** (1966) 1156; F. Englert and R. Brout, Phys. Rev. Lett. **13** (1964) 321; G. S. Guralnik, C. R. Hagen and T. W. Kibble, Phys. Rev. Lett. **13** (1964) 585; T. W. B. Kibble, Phys. Rev. **155** (1967) 1554.

[2] The ATLAS Collaboration, Phys. Lett. **B716** (2012) 1 [arXiv:1207.7214]; The CMS Collaboration, Phys. Lett. **B716** (2012) 30 [arXiv:1207.7235].

[3] A. Djouadi *et al.*, hep-ph/9901246.

[4] A. Arbey, M. Battaglia, A. Djouadi, F. Mahmoudi, M. Muhlleitner and M. Spira, Phys. Rev. D **106** (2022) no.5, 055002 [arXiv:2201.00070].

[5] M. S. Carena, D. Garcia, U. Nierste and C. E. M. Wagner, Nucl. Phys. **B577**, 88 (2000) [hep-ph/9912516].

[6] J. Guasch, P. Häfliger and M. Spira, Phys. Rev. **D68**, 115001 (2003) [hep-ph/0305101].

[7] J. de Blas, M. Cepeda, J. D'Hondt, R. K. Ellis, C. Grojean, B. Heinemann, F. Maltoni, A. Nisati, E. Petit, R. Rattazzi and W. Verkerke, JHEP **01** (2020), 139 [arXiv:1905.03764].

[8] A. Arbey, M. Battaglia and F. Mahmoudi, Eur. Phys. J. C **72** (2012) 1847 [arXiv:1110.3726]; Phys. Rev. D **89** (2014) no.7, 077701 [arXiv:1311.7641]; Phys. Rev. D **94** (2016) no.5, 055015 [arXiv:1506.02148].

[9] F. Mahmoudi, Comput. Phys. Commun. **178** (2008) 745 [arXiv:0710.2067]; Comput. Phys. Commun. **180** (2009) 1579 [arXiv:0808.3144]; Comput. Phys. Commun. **180** (2009) 1718.

[10] B. C. Allanach, Comput. Phys. Commun. **143** (2002) 305 [hep-ph/0104145].

[11] A. Djouadi, J. Kalinowski and M. Spira, Comput. Phys. Commun. **108** (1998) 56 [hep-ph/9704448]; A. Djouadi, J. Kalinowski, M. Muehlleitner and M. Spira, Comput. Phys. Commun. **238** (2019), 214 [arXiv:1801.09506].

[12] A. Arbey and F. Mahmoudi, Comput. Phys. Commun. **181** (2010) 1277 [arXiv:0906.0369]; Comput. Phys. Commun. **182** (2011), 1582.

[13] A. Djouadi, Phys. Rept. **459** (2008) 1 [hep-ph/0503173].

[14] The ATLAS collaboration, ATL-CONF-2021-053.

[15] The CMS Collaboration, CMS-PAS-HIG-19-005.

[16] The CMS Collaboration, Phys. Lett. **B793** (2019), 520 [arXiv:1809.05937].

[17] The ATLAS Collaboration, Phys. Rev. Lett. **122** (2019) no.23, 231801 [arXiv:1904.05105].

[18] The ATLAS Collaboration, ATLAS-CONF-2020-008.

[19] The ATLAS Collaboration, ATLAS-CONF-2020-052.

[20] E. Aprile *et al.* [XENON], Phys. Rev. Lett. **121** (2018) no.11, 111302 [arXiv:1805.12562].